Ultrasensitive Chemical Sensing through Facile Tuning Defects and Functional Groups in Reduced Graphene Oxide

ARTICLE *in* ANALYTICAL CHEMISTRY · JULY 2014

Impact Factor: 5.64 · DOI: 10.1021/ac501274z · Source: PubMed

8 AUTHORS, INCLUDING:

Shumao Cui
University of Wisconsin - Milwaukee
64 PUBLICATIONS **1,510** CITATIONS
SEE PROFILE

Eric C Mattson
University of Wisconsin - Milwaukee
38 PUBLICATIONS **461** CITATIONS
SEE PROFILE

Zhenhai Wen
University of Wisconsin–Madison
90 PUBLICATIONS **2,723** CITATIONS
SEE PROFILE

Jingbo Chang
University of Wisconsin - Milwaukee
49 PUBLICATIONS **576** CITATIONS
SEE PROFILE

analytical chemistry

Article

pubs.acs.org/ac

Ultrasensitive Chemical Sensing through Facile Tuning Defects and Functional Groups in Reduced Graphene Oxide

Shumao Cui,[†] Haihui Pu,[†] Eric C. Mattson,[‡] Zhenhai Wen,[†] Jingbo Chang,[†] Yang Hou,[†] Carol J. Hirschmugl,[‡] and Junhong Chen*[,†]

[†]Department of Mechanical Engineering, University of Wisconsin-Milwaukee, Milwaukee, Wisconsin 53211, United States

[‡]Department of Physics, University of Wisconsin-Milwaukee, Milwaukee, Wisconsin 53211, United States

Supporting Information

ABSTRACT: Herein, we report on a facile, low-cost, and efficient method to tune the structure and properties of chemically reduced graphene oxide (rGO) by applying a transient voltage across the rGO for ultrasensitive gas sensors. A large number of defects, including pits, are formed in the rGO upon the voltage activation. More interestingly, the number of epoxide and ether functional groups in the rGO increased after the voltage activation. The voltage-activated rGO was highly sensitive to NO_2 with a sensitivity 500% higher than that of the original rGO. The lower detection limit can reach an unprecedented ultralow concentration of 50 ppb for NO_2 sensing. Density functional theory (DFT) calculations revealed that the high sensitivity to NO_2 is attributed to the efficient charge transfer from ether groups to NO_2, which is the dominant sensing mechanism. This study points to a promising method to tune the properties of graphene-based materials through the creation of additional defects and functional groups for high-performance gas sensors.

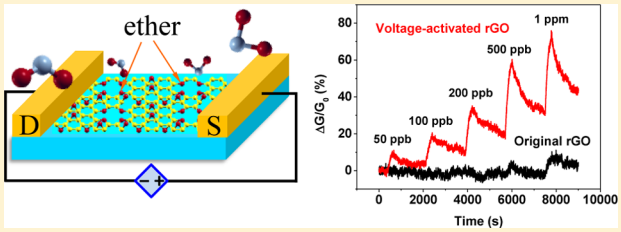

Graphene is a promising material for electronic devices due to its unique properties;[1,2] various exciting applications of graphene have been demonstrated, including gas sensors,[3,4] biosensors,[5] and energy devices.[6,7] Generally, graphene-based gas sensors have the advantages of high sensitivity, low-noise level, and low power consumption.[4] However, it remains a challenge to achieve an exceptional sensitivity allowing for the detection of toxic gases at concentrations of a low parts per billion (ppb) level, which are important for industrial, environmental, and military applications.

Previous work has reported that defect sites with oxygen groups in single-walled carbon nanotubes dominated the sensing response and can be used to enhance the sensitivity.[8] Indeed, steam-etched porous graphene oxide (GO) with abundant defect sites, including large vacancies (i.e., holes), has been shown to have more enhanced interactions with NO_2, which is a toxic pollutant and has been extensively studied as a model analyte for graphene-based sensing materials.[9−11] Therefore, tuning the defects and oxygen functional groups in graphene-based materials is a promising method to significantly enhance the sensing response of graphene-based gas sensors.

In this work, we report a facile, low-cost, and efficient method to tune the structure and properties of reduced graphene oxide (rGO) by applying a voltage across the rGO for a short duration in a room air environment (Figure 1a). We found that the rGO was greatly activated by creating more active defects and oxygen functional groups for gas adsorption, and as a result, the sensing performance of rGO was significantly improved. On the basis of our data, the lower detection limit of our voltage-activated rGO to NO_2 can reach a very low concentration of 50 ppb, which is much lower than any other rGO-based sensor reported so far. The method also can be used to dope various elements in the graphene basal plane to further expand rGO applications. Density functional theory (DFT) calculations were carried out to understand the

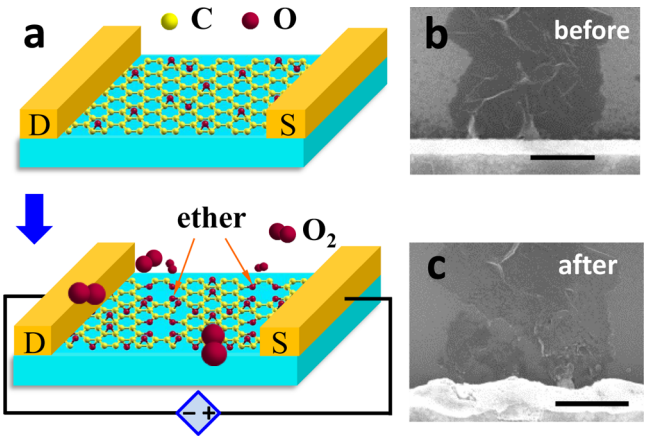

Figure 1. (a) Schematic illustration of the voltage activation process for rGO in the air. After the voltage-activation process, more defects and oxygen functional groups (epoxide and ether groups) form in the rGO. (b, c) SEM images of rGO before and after the voltage activation, respectively. The scale bars in (b) and (c) are 0.5 μm.

Received: April 8, 2014
Accepted: July 3, 2014
Published: July 3, 2014

   dx.doi.org/10.1021/ac501274z | Anal. Chem. 2014, 86, 7516−7522

sensing mechanisms of the defects and oxygen funcional groups.

EXPERIMENTAL SECTION

Synthesis of rGO. The rGO was obtained by chemically reducing a diluted commercial single layer GO water dispersion (ACS Material) using our previously reported method.[9] Briefly, $H_3NO{\cdot}HCl$ (0.5 g) was added into 25 mL of GO dispersion (1 mg/25 mL) and the mixture was continuously stirred at 80 °C for 30 h. The black product was filtered and rinsed by DI water and acetone to obtain rGO powders. Then, the rGO powder was dispersed in *N*,*N*-dimethylformamide (DMF) with sonication for 2 h.

Fabrication of Sensor Devices. The sensor device was fabricated by drop casting the rGO dispersion onto interdigitated gold electrodes. The gold electrodes were fabricated using e-beam lithography on a silicon substrate with a thin SiO_2 top layer. A tiny drop (1 μL) of the rGO dispersion (0.05 mg/mL) was drop cast on the gold electrodes, followed by drying in air, leading to rGO nanosheets bridging the gold fingers. Further annealing was carried out at 200 °C for 1 h in an Ar atmosphere to remove the residual DMF and improve contacts between rGO and gold fingers.

Voltage Activation Process and Characterization. Various DC voltages were sequentially applied across the electrodes in air to investigate the rGO structural changes and their influence on the sensing performance. The morphology of the rGO on the sensing devices was characterized by scanning electron microscopy (SEM) (Hitachi S-4800). Transmission infrared (IR) microspectroscopy measurements were performed at the Synchrotron Radiation Center using the Infrared Environmental Imaging (IRENI) beamline[12] to examine the variation of oxygen functional groups in the rGO.

Sensing Tests. The rGO sensor device was placed in an airtight chamber with electrical feedthroughs. A constant voltage was applied to the device. The variation of resistance was monitored and recorded with the changes in the gas environment using a Keithley 2602 source meter. Typically, a sensing-measurement cycle has three continuous steps: (1) introducing dry air (2 $Lmin^{-1}$) as a background, (2) then injecting an analyte gas (2 $Lmin^{-1}$) to register a sensing signal, and (3) introducing dry air (2 $Lmin^{-1}$) again for sensor recovery.

Density Functional Theory (DFT) Calculation Method. To further understand the sensing mechanism, DFT calculations were implemented using OPENMX.[36] The pseudoatomic orbitals (PAOs) within the framework of norm-conserving pseudopotentials were used, and the exchange-correlation functional was treated in the formalism of the local spin density approximation (LSDA) for NO_2. The basic functions were specified by two primitive orbitals of individual s and p orbitals with the cutoff atomic radius of 7.0 in Bohr for all elements considered. A single molecular adsorbate was put in the 3 × 3 supercell composed of a centered rectangular unit cell of graphene, and the layer spacing was set to be larger than 20 Å in order to minimize the interactions between the adjacent layers and between the molecules themselves. A cutoff energy of 200 Ry in real space and a k-point density of 0.02/Å in reciprocal space were used for the numerical integrations. The structural optimizations stopped when the force was less than 0.01 eV/Å between the successive iterations.

RESULTS AND DISCUSSION

Figure 1b,c shows SEM images of the same rGO area before and after being activated using step-increasing voltages up to 40 V in a room air environment. The voltage interval was 5 V, and each step lasted for 1 min (Figure S1, Supporting Information). Compared with the original rGO (Figure 1b), the morphology had a significant change with some breakdown regions, as shown in Figure 1c. The locations of the failure area are both near the contact region with gold electrodes and in the middle of the gap, similar to the breakdown locations on current-passing graphene.[13] This sheds light on the breakdown mechanism of Joule heating. It has been reported that abundant defects in GO or rGO are very active upon heating while being exposed to air, resulting in uniformly distributed etch pits throughout the entire flakes.[11] Here, a similar result was obtained in our rGO upon the heating induced by the voltages. The etching is well evidenced by the SEM images in Figure 1. Thermal annealing of rGO could lead to similar products, which was further confirmed through controlled experiments of thermally treating rGO exposed to air using a tube furnace at a temperature of 200−450 °C for a short duration (Supporting Information). According to the SEM images upon the heating experiments (Figure S2, Supporting Information), the edges (white arrows) and central areas (red circles) of rGO were severely etched at 450 °C, leading to a large number of edges and defects. This also can be well observed from SEM images with a higher magnification (Figure S3, Supporting Information).

The electrical properties of rGO were studied before and after the voltage (V_t) activation in air (Figure 2). Figure 2a shows the $I-V$ characteristics of rGO after the activation by different V_t. The voltages were applied on the rGO sequentially from low to high, and each V_t lasted for 1 min. The resistance

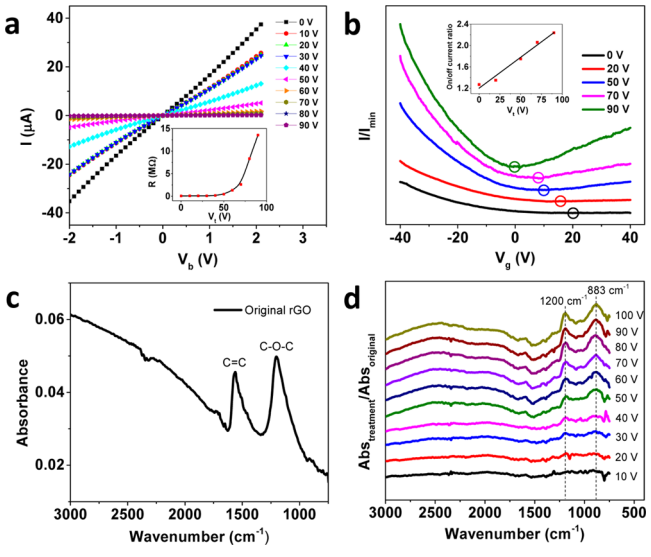

Figure 2. (a) $I-V$ characteristics of rGO sheets after activation in the air under various voltages (V_t) with an interval of 10 V. Inset: Electrical resistance (R) of rGO vs V_t. (b) Evolution of FET characteristics of rGO with activation of V_t. Inset: On/off current ratio vs V_t. (c) IR absorption spectrum of original rGO. The primary functional groups on the rGO surface are epoxide groups (C−O−C asymmetric and symmetric stretching, 1200 cm^{-1}). (d) Differential IR absorption spectra of voltage-activated rGO, indicating increases in epoxide (1200 cm^{-1}) and ether (883 cm^{-1}) groups after voltage activation.

dx.doi.org/10.1021/ac501274z | Anal. Chem. 2014, 86, 7516−7522

of the rGO gradually increased with the increase of V_t. The inset in Figure 2a shows the resistance evolution curve with the rate of resistance increase accelerating at 40 V, which is attributed to the large Joule heating at higher voltages that led to more defects such as holes. For some samples, there was a limited decrease in resistance during the first few voltage applications, followed by subsequent increases in resistance with further voltage application (Figure S4, Supporting Information). The thermally treated rGO (in the air) also showed similar $I-V$ characteristics and consistent resistance changes (Figure S5a, Supporting Information). By comparing the curve of resistance versus voltage (inset of Figure 2a) with that of resistance versus temperature (inset of Figure S5a, Supporting Information), we can estimate the critical temperatures of the sample for Figure 2. A combined chart is plotted in Figure S5b, Supporting Information, and according to the related resistance change, it is clear that there is no obvious resistance change until 40 V is applied. Thus, the temperature of the rGO can be estimated to be about 400 °C at 30 V. After 40 V is applied, the rGO can reach about 450 °C, leading to a dramatic resistance increase.

On the basis of previous studies, thermal reduction of GO in an inert atmosphere (argon or vacuum) causes a decrease in resistance.[10,14] It is expected that thermal treatment can partially remove the oxygen functional groups from the GO surface, leading to more graphitic areas and a higher electrical conductivity. However, in this work, the conductance changed in an opposite direction (decreased). For example, the original rGO had a resistance of 6.1×10^4 Ω, but after activation at 90 V, the resistance increased to 1.4×10^7 Ω, which is 3 orders of magnitude higher than the original resistance. Therefore, the structural change of our rGO (including oxygen functional groups and basal plane) is significantly different from conventional rGO after thermal or chemical reduction of oxygen functional groups.

To observe the change in oxygen functional groups, rGO was characterized using IR microspectroscopy before and after the voltage activations. Figure 2c shows the IR absorption spectrum of the original rGO. The band at 1562 cm^{-1} is assigned to the C═C stretch of the graphene lattice, while the band at 1200 cm^{-1} is attributed to the asymmetric and symmetric stretching modes of epoxide groups.[15] There are no other significant absorption bands observed in the spectrum. The evolution of the differential IR spectra of the rGO from exactly the same position on the sample following sequential voltage activations is shown in Figure 2d. The bands in the 800−1300 cm^{-1} region can be assigned to residual epoxide and cyclic ether oxygen functional groups. In addition to the assignment of epoxide groups to the 1050−1300 cm^{-1} region,[15] previous studies found that edge terminations of cyclic ether groups produced collective modes in the lower frequency (800−1000 cm^{-1} regions).[16] While the frequency of these collective C−O−C stretching modes is ultimately determined by the lateral size of the exposed edge (higher vibrational frequency with decreasing edge length), the substantial degree of burning resulting from the voltage activation could easily expose large edge-domain sizes that rapidly become oxidized in the air. As the applied voltage increased from 10 to 100 V, a substantial increase in the intensity of epoxide (1200 cm^{-1}) and ether (883 cm^{-1}) groups was observed. These data demonstrate that the voltage activation facilitated the formation of oxygen functional groups (epoxy and ether groups) in rGO likely due to the reaction between the oxygen in the air and the carbon atoms of the rGO at a high temperature.[17,18] The significant rise of cyclic ether groups also reveals the increase of defects after the voltage activation. On the basis of the above data, the voltage-activation process is proved to be an oxidation process instead of a reduction process commonly observed for the conventional chemical/thermal reduction of rGO.[10,19]

Although the increase of oxygen functional groups may also cause a resistance increase of rGO due to the effect of sp^3 carbon bonds,[20] we believe that the additional defects dominate the resistance increase in this work because a dramatic resistance change can only occur with the creation of a large number of defects. This speculation was confirmed through controlled experiments by adding a gradual step-increasing voltage to the rGO until it was completely broken down. Figure S6, Supporting Information, shows the current versus time curve of the sequential voltage application. The rGO resistance did not show an obvious change until the applied voltage reached 15 V, which caused a sudden increase in the electrical resistance. The resistance kept increasing for a voltage up to 20−22 V, and the breakdown occurred at the end of 22 V. The corresponding structure change was captured (Figure S7, Supporting Information). After being maintained at 15 V for 1 min, some defects appeared on the suspending rGO near the contacts with the gold electrodes (Figure S7b and inset, Supporting Information). Considering the sudden increase of resistance, the defects are likely responsible for the dramatic resistance increase. With a higher voltage (20 V), more defects near the electrode contacts were induced (Figure S7c, Supporting Information), leading to another dramatic resistance increase. This defect-induced resistance increase is also consistent with that of thermally treating rGO (Figures S2, S3, and S5a, Supporting Information).

The structural change of rGO also significantly affects its field-effect transistor (FET) properties. Figure 2b shows the evolution of the rGO FET characteristics before and after four V_t activations. We measured the current-gate voltage (V_g) curve immediately after each V_t activation. To normalize the curves, the Y axis represents the ratio of current (I) to the minimum current (I_{min}) at Dirac points. The $I/I_{min}-V_g$ curves show that the Dirac point gradually shifted from a V_g of ∼20 V for the original rGO to a V_g of 0 V for the rGO after being treated with a V_t of 90 V, indicating the removal of the p-doping sources.[21,22] Although the oxygen functional groups increased on the basis of the IR data, a large number of other p-doping sources from the air (e.g., physisorbed oxygen molecules) were removed. Those p-doing sources strongly induce p-type behavior of rGO even for n-doped rGO.[23] Previous studies showed that chemical doping on graphene only rigidly shifts the Dirac point without any significant change in the V shape of the conductivity-gate voltage curve.[4] However, the shape of FET curves in Figure 2b becomes sharper and the electron transport is enhanced with the increasing V_t, further confirming the removal of extrinsic p-doping sources. Meanwhile, the on/off current ratio (I_{on}/I_{off}) increased with the increasing V_t, and it can be well fitted by a linear line as shown in the inset of Figure 2b. For narrow graphene or graphene nanoribbons (GNRs), the bandgap (E_g) can be estimated by $I_{on}/I_{off} \propto \exp(E_g/k_BT)$ (where k_B is the Boltzmann constant and T is the temperature) and the $I_{on}/I_{off} \propto 1/w$ (w is the width of GNRs).[24] In this study, all the FET measurements were conducted at room temperature. Therefore, our results suggest the bandgap of our rGO increases with increasing V_t and can be tuned by the voltage activation. However, further investigation is needed to confirm

dx.doi.org/10.1021/ac501274z | Anal. Chem. 2014, 86, 7516−7522

the bandgap tuning. Although the n-type transport in the rGO was enhanced after the voltage activations,[25] the p-type transport was still stronger than the n-type transport, likely due to the intrinsic p-type doping sources (epoxide and ether groups) on the rGO.

Nitrogen dioxide (NO_2) was selected to evaluate the sensing performance of our voltage-activated rGO. The voltage application curves are shown in Figures 3a and S8, Supporting Information. Each V_t was applied for 1 min with a base voltage of 0.5 V. The rGO showed a significant conductance drop after a voltage of 25 V was applied, suggesting the formation of a large number of defects. The sensing performance was evaluated against 100 ppm of NO_2 for the original rGO and the rGO after being activated with V_t ≥25 V. The sensor sensitivity was defined as $S = \Delta G/G_0$, where ΔG is the change in conductance before and after gas exposure and G_0 is the average conductance before the gas exposure. Figure 3b shows the responses of rGO before and after voltage activations. Because of the p-type semiconducting behavior of rGO and the oxidizing NO_2 that can withdraw electrons from rGO, all the sensor devices showed an increased conductivity upon exposure to NO_2.[9−11] The sensitivity of the original rGO was 36%. For the voltage-activated rGO, however, the sensitivity gradually increased to 180%, which is five times that of the original rGO.

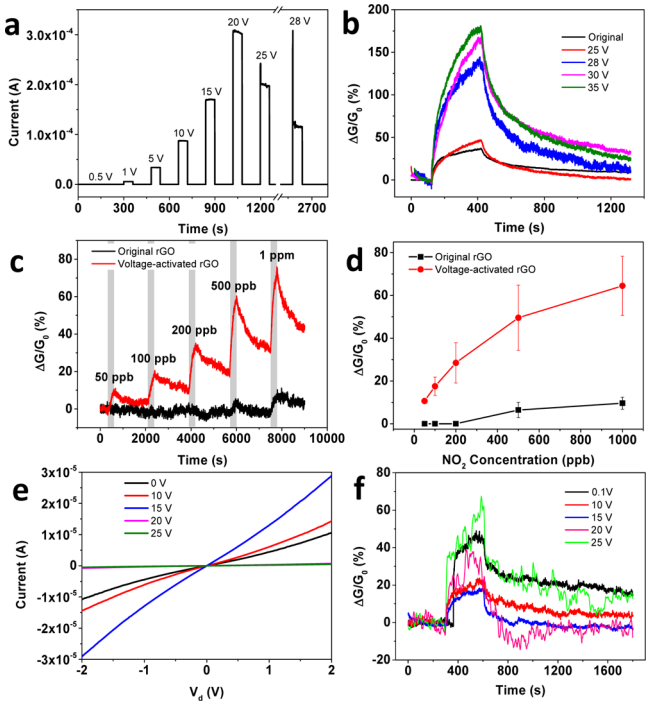

Figure 3. (a) Current−time profile with V_t applied on rGO; V_t ranges from 1 to 28 V (1 min duration) with a base voltage of 0.5 V. (b) Sensing responses of the original rGO and voltage-activated rGO toward 100 ppm of NO_2 with a bias voltage of 0.5 V. (c) Sensing response versus time for an rGO sensor before and after activation with voltages up to 28.6 V upon exposure to NO_2 gas with concentrations ranging from 50 ppb to 1 ppm. The bias voltage during the sensing measurements was 0.2 V. (d) Sensitivity comparison for the rGO sensors. (e, f) $I-V$ characteristics of an rGO sensor device treated with various voltages in an Ar atmosphere and the sensing performance evolution toward 100 ppm of NO_2, respectively. The sensing bias voltage was in a range of 0.03−0.7 V to keep the device in an appropriate working condition.

The highest sensitivity corresponded with the highest V_t, which was likely due to the highest concentration of defects and oxygen functional groups (Figure 2d). For the original rGO, it took overnight to recover to its initial state; however, the voltage-activated rGO fully recovered within 1 h, which is likely related to the high defect density in the rGO.[11]

Similarly, the sensitivity of the thermally treated rGO also gradually increased with increasing temperature and longer duration (Figure S9, Supporting Information). The largest increase in the sensitivity occurred in the heating duration from 1 to 2 min at 450 °C, where the resistance had the largest increase with a large number of defects created (Figures S3 and S5, Supporting Information). Furthermore, the defects are very reactive to adsorbed O_2 to form oxygen functional groups (i.e., ether groups).[26] Therefore, it is reasonable to conclude that defects with ether groups dominate the sensing response. Moreover, this activated rGO can be used as an enhanced sensing layer in thick rGO film sensors. We thermally treated a thick rGO film (~50 nm) at 450 °C for 2 min in air. It is clear that the top layer was seriously etched with the treatment (Figure S10a,b, Supporting Information). However, the inner layers kept their original status due to the protection of the top layers. The sensing performance of the thick rGO film to 100 ppm of NO_2 shows that the sensitivity was greatly enhanced after the treatment due to the enhancement of the top sensing layer (Figure S10c, Supporting Information). However, the sensitivity is still much lower than that of the single- or few-layer rGO sensors treated under the same condition. The possible reason is that the treated rGO with defects has better semiconducting properties than the original rGO, leading to a better response than that of the original rGO as the conductance channel.

To further investigate the removal of extrinsic p-doping sources through voltage activation, the same device (after voltage activation of 35 V) was exposed to a room air environment for 2 weeks to adsorb p-type doping sources from the air. It was found that any short exposure of rGO to the room environment lead to dramatic p-type doping.[27] In addition, electrical properties of the device were characterized (Figure S11a,b, Supporting Information), and the sensing response of the device to 100 ppm of NO_2 was measured. It was found that the sensitivity further increased to about 200% (Figure S11c, Supporting Information). The adsorbed p-type doping sources are very likely responsible for this increase in response. Furthermore, the recovery time of the device was prolonged to overnight. To remove the dopants, a voltage of 35 V was applied to the rGO again for 1 min to activate the removal of p-dopants without significant modification of the rGO structure. Because the voltage had already been applied to the rGO once, part of the rGO was burned, accompanied by the increase of resistance. Here, with the same voltage and a much lower current passing through the rGO, the relatively small Joule heating can only lead to the desorption of some physisorbed p-doping sources without further burning the rGO. Indeed, the electrical conductivity of the device increased due to the recovery of graphitic areas (Figure S11a, Supporting Information). The desorption of p-type dopants also caused the Dirac point to shift negatively (Figure S11b, Supporting Information), which is consistent with the results in Figure 2b.

The voltage activation can also significantly enhance the lower detection limit of rGO sensors. Figure 3c shows the responses of an rGO sensor before and after voltage activations (up to 28.6 V) upon exposure to different concentrations of

dx.doi.org/10.1021/ac501274z | Anal. Chem. 2014, 86, 7516−7522

NO_2 with the sensitivity comparison shown in Figure 3d. For the original rGO, a distinguishable response showed up only for a concentration of 1 ppm. However, a sensitivity of 74% was observed for the voltage-activated rGO for 1 ppm of NO_2 with a short exposure time of 5 min. The voltage-activated rGO even can respond to a NO_2 concentration as low as 50 ppb with a sensitivity of 10%. On the basis of a signal (S)-to-noise (N) ratio S/N > 3, 50 ppb can be considered as the new lower detection limit of our rGO, which is superior to other high-performance rGO-based NO_2 gas sensors. For example, the calculated lower detection limits of rGO conjugated with Cu_2O nanowires and chemically modified rGO are 64 and 70 ppb, respectively.[28,29] The lower detection limit reported here is even comparable with the calculated lower detection limit of single-walled carbon nanotubes (SWNTs) to NO_2 (44 ppb).[30] The same sensor was exposed to 1 ppm of NO_2 for multiple successive cycles as shown in Figure S12, Supporting Information. Consistent sensing responses were observed, indicating the excellent repeatability of our sensor. However, the sensor needs a relatively long time to recover to its initial state, leading to a baseline drift. This is likely due to the relatively strong binding between the sensing material and the gas molecules, and an inert gas or UV light can facilitate the recovery.[29,30] The baseline drift of the sensing curve can also be suppressed with a longer recovery time (Figure S12, Supporting Information).

The same rGO was treated in an Ar atmosphere to examine the effect of activation atmosphere on the oxygen functional groups, stimulated defects, and gas sensing performance. Since the Ar atmosphere is an inert environment, it is anticipated that oxygen functional groups on rGO could be effectively reduced by the electrothermal heating without significantly damaging the graphene basal plane.[10] Indeed, the electrical conductivity of the rGO had a significant increase before partial breakdown occurred (here at 20 V for this device) due to the recovery of the graphitic basal plane (Figure 3e), which is different from the case in a room air environment. After the partial breakdown at 20 V, the resistance of the rGO greatly increased. The morphology was observed after the complete breakdown at 30 V. It was found that narrow cracks in rGO only appeared in the middle of the electrode gap (Figure S13, Supporting Information). Therefore, the defect area was smaller than that for the rGO exposed to air. The sensing performance was measured against 100 ppm of NO_2 after each treatment step. The sensing results (Figure 3f) show that the sensitivity decreased with the removal of oxygen functional groups. Upon breaking down after the 20 V treatment, the sensitivity gradually increased until the complete breakdown, at which point the sensitivity was comparable with that of the original rGO. A parallel sample treated in Ar was also measured using IR microspectroscopy, and there were no additional oxygen functional groups formed on the basis of the data (Figure S14, Supporting Information). Therefore, we conclude that both oxygen functional groups and defects can help to improve the sensitivity of rGO. However, existing oxygen groups were removed, and no additional oxygen groups were created when the rGO was heated in an inert atmosphere. The number of defects for the rGO treated in Ar was also less than that of the rGO activated in the air environment due to the creation of a smaller number of cracks in the rGO.

Ammonia has been found quite reactive at the edge of graphene and has been used as a source to produce N-doping graphene.[22] This is attributed to the fact that NH_3 molecules adsorbed on defect sites are dissociated into NH_2 and H that are then bonded to carbon atoms.[31] To further confirm the sensing enhancement of the voltage-activated rGO, an rGO device was exposed to 1% NH_3 before and after V_t activation and the sensing response is shown in Figure S15, Supporting Information, where the sensitivity is defined as $\Delta R/R$ (ΔR: the resistance change of rGO before and after NH_3 exposure; R: rGO resistance in air before NH_3 exposure). The sensitivity increased with the increasing V_t, and a dramatic increase in sensitivity started at 10 V, suggesting a substantial structure change in the rGO after being treated with V_t > 10 V. However, the sensor had a slow recovery process, likely due to the irreversible NH_3 molecule dissociation at defects. This experiment suggests a facile method to dope graphene with selected dopants (e.g., N, S, and Cl) in a designed gas environment through voltage activation.

To show a typical example, the NH_3 atmosphere was selected to dope N in the rGO using our voltage activation method. The same voltage-activation process was carried out in a gas environment of pure NH_3 instead of air. Each voltage treatment lasted for 1 min, and the electrical properties were measured after the treatments under N_2 protection to examine the doping effect (Figure 4a,b). As shown in Figure 4b, the original rGO

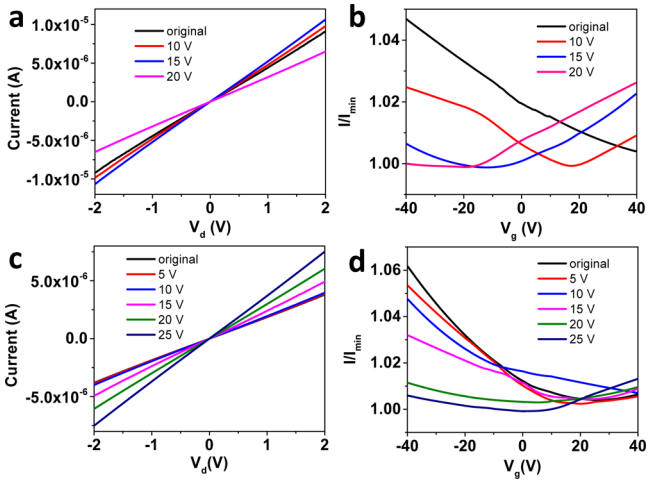

Figure 4. (a) $I-V$ characteristics of an rGO device before and after voltage activations in an NH_3 gas and (b) the corresponding FET characteristics. The voltage activation duration was 1 min for each voltage. After the activation, the electrical properties were measured immediately under N_2 protection. (c) $I-V$ characteristics of an rGO device before and after voltage treatments in N_2 gas and (d) the corresponding FET characteristics. All the measurements were under N_2 protection. This device reached breakdown at 30 V.

showed highly p-type semiconducting behavior and the Dirac point was at a V_g much higher than 40 V. However, after activation at 20 V, the Dirac point negatively shifted to a V_g of −20 V and the rGO showed a very weak p-type transport but a strong n-type transport, indicating the successful N doping in rGO.[22] To further confirm the N-doping, the same rGO was voltage treated using the same process in a pure N_2 atmosphere. However, the Dirac point remained at a positive V_g until the device reached breakdown (Figure 4d).

It is well-known that gas molecules tend to adsorb to sites with a larger binding energy. For each type of adsorption site (e.g., ether groups) on the rGO, the Langmuir equation can be adopted to estimate the coverage θ_i at equilibrium:

dx.doi.org/10.1021/ac501274z | Anal. Chem. 2014, 86, 7516−7522

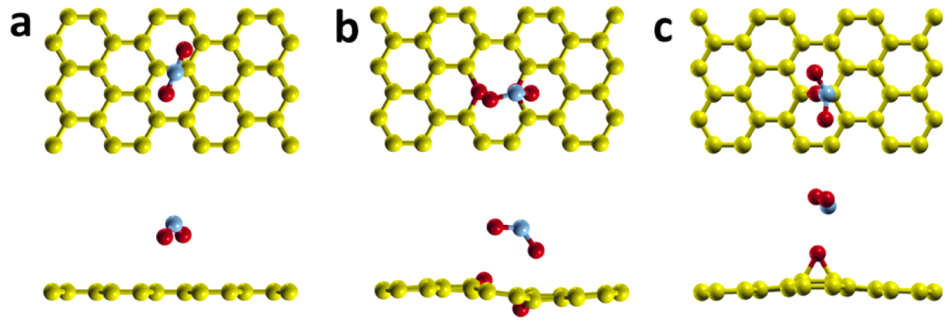

Figure 5. Top (upper panel) and side (lower panel) views of gas adsorption on different sites of rGO: (a) NO_2 on sp^2 carbon, (b) NO_2 on ether groups, and (c) NO_2 on epoxide groups in rGO. The yellow, red, and light blue balls represent carbon, oxygen, and nitrogen atoms, respectively.

$$\theta_i = \frac{K_{e,i}C_g}{1 + K_{e,i}C_g} \tag{1}$$

and

$$C_g = \frac{P_g}{P_{air}}C_{air} \tag{2}$$

where P_g is the partial pressure of the target gas; P_{air} is the air pressure; C_{air} is a constant (2.9×10^8 m^{-1}) for air at room temperature; $K_{e,i}$ is the equilibrium constant that is defined as the ratio of the classical adsorption rate constant $K_{a,c} = (k_BT/2\pi m_g)^{1/2}$ to the classical desorption rate constant $K_{d,c} = \omega_g \exp(-(E_b/(k_BT))/2\pi$,[32] where $\omega_g = \gamma(2E_b/m_g)^{1/2}$ is the characteristic frequency of gas molecules with mass m_g;[33] k_B is the Boltzmann constant; and γ is the fitting parameter in the Morse potential. The exact value of $K_{e,i}$ depends on γ from fitting the Morse potential; however, γ has been fitted to be around 1.5 $Å^{-1}$ for gas adsorption on different sites, and $K_{e,i}$ can thus be expressed as a function of binding energy $E_{b,i}$ alone with a high accuracy,

$$K_{e,i} = \frac{K_{a,c}}{K_{d,c}} \approx \sqrt{\frac{k_BT}{E_{b,i}}}\exp\left(\frac{E_{b,i}}{k_BT}\right) \times 1.2 \times 10^{-10}\text{m} \tag{3}$$

To obtain the binding energies and to further understand the sensing enhancement by the voltage activation, DFT calculations were performed for gas adsorption on sp^2 carbon, ether groups, epoxide groups, and defects without oxygen. For the simulation, a single gas molecule is placed near the adsorption site and allowed to relax until it reaches the minimum potential. The optimized structures are shown in Figure 5. The binding energy of a single gas molecule is calculated as $E_b = E_{rGO} + E_{gas} - E_{rGO+gas}$, where E_{rGO}, E_{gas}, and $E_{rGO+gas}$ are the energies of the rGO, the isolated gas molecule, and the rGO-gas system. The results show that the binding energy is 0.371, 0.212, and 0.545 eV for NO_2 adsorbed on the sp^2 carbon, the epoxide group, and the ether group, respectively. For the defects, NO_2 will be dissociated into NO molecule and atomic O atoms bonded to the dangling C atom forming carbonyl (Figure S16, Supporting Information). However, the defects are very reactive to dissociate the O_2 molecules into ether groups for the lowest energy structures; i.e., the defects only appear with oxygen groups on them in the air environment.[26] From eqs 1 to 3 for 1 ppm of NO_2 diluted in air at room temperature, we found that the coverage is 0.92 for NO_2 on the ether groups. Compared with the coverage of 0.016×10^{-2} for NO_2 adsorbed on the aromatic carbon atoms and 4.65×10^{-5} on the epoxides, ether groups in rGO are very reactive and can greatly enhance the adsorption of NO_2. Together with the experimental results, we can conclude that the ether groups dominate the sensing response to NO_2. The enhanced sensitivity of NO_2 is due to the potential charge transfer from the ether to NO_2 with the oxygen atoms in NO_2 pointing toward ether, which is unlike the case of forming the NO_3 complex between NO_2 and carbonyl at the edge of rGO or between NO_2 and oxygen atoms at the surface of metal oxides.[34,35]

CONCLUSIONS

In summary, transient high voltage activation on rGO can deeply remove extrinsic p-doping sources from air, increase oxygen functional groups (epoxide and ether groups), and create a large number of defects in rGO, leading to significant changes in electrical properties of rGO such as electrical conductivity and FET behavior. Compared with the original rGO, the voltage-activated rGO shows significantly enhanced sensing responses to both NO_2 and NH_3. The lower detection limit of the voltage-activated rGO to NO_2 can reach an ultralow concentration of 50 ppb. The ether groups are primarily responsible for the ultrahigh sensing response to NO_2. The method also can be used to dope various elements (e.g., N, S, and Cl) in rGO. This study suggests a facile and effective method to fabricate high-performance graphene-based gas sensors through in situ modulation of rGO properties using transient voltages.

ASSOCIATED CONTENT

Supporting Information

More experimental details, SEM images, electrical properties, and sensing responses. This material is available free of charge via the Internet at http://pubs.acs.org.

AUTHOR INFORMATION

Corresponding Author

*E-mail: jhchen@uwm.edu.

Notes

The authors declare no competing financial interest.

ACKNOWLEDGMENTS

Financial support for this work was provided by the US National Science Foundation (IIP-1128158) and University of Wisconsin-Milwaukee Research Foundation Bradley Catalyst Grant. The authors thank Prof. M. Gajdardziska-Josifovska for TEM access at the UWM HRTEM Laboratory and Dr. H. A. Owen for technical support with SEM analyses. The SEM

imaging was conducted at the UWM Electron Microscope Laboratory.

REFERENCES

(1) Avouris, P. *Nano Lett.* **2010**, *10*, 4285.
(2) Geim, A. K.; Novoselov, K. S. *Nat. Mater.* **2007**, *6*, 183.
(3) Cui, S. M.; Mao, S.; Lu, G. H.; Chen, J. H. *J. Phys. Chem. Lett.* **2013**, *4*, 2441.
(4) Schedin, F.; Geim, A. K.; Morozov, S. V.; Hill, E. W.; Blake, P.; Katsnelson, M. I.; Novoselov, K. S. *Nat. Mater.* **2007**, *6*, 652.
(5) Mao, S.; Lu, G. H.; Yu, K. H.; Bo, Z.; Chen, J. H. *Adv. Mater.* **2010**, *22*, 3521.
(6) Wang, X.; Zhi, L. J.; Mullen, K. *Nano Lett.* **2008**, *8*, 323.
(7) Xiao, J.; Mei, D. H.; Li, X. L.; Xu, W.; Wang, D. Y.; Graff, G. L.; Bennett, W. D.; Nie, Z. M.; Saraf, L. V.; Aksay, I. A.; Liu, J.; Zhang, J. G. *Nano Lett.* **2011**, *11*, 5071.
(8) Robinson, J. A.; Snow, E. S.; Badescu, S. C.; Reinecke, T. L.; Perkins, F. K. *Nano Lett.* **2006**, *6*, 1747.
(9) Mao, S.; Yu, K. H.; Cui, S. M.; Bo, Z.; Lu, G. H.; Chen, J. H. *Nanoscale* **2011**, *3*, 2849.
(10) Lu, G. H.; Ocola, L. E.; Chen, J. H. *Appl. Phys. Lett.* **2009**, *94*, 083111.
(11) Han, T. H.; Huang, Y. K.; Tan, A. T. L.; Dravid, V. P.; Huang, J. X. *J. Am. Chem. Soc.* **2011**, *133*, 15264.
(12) Nasse, M. J.; Walsh, M. J.; Mattson, E. C.; Reininger, R.; Kajdacsy-Balla, A.; Macias, V.; Bhargava, R.; Hirschmugl, C. J. *Nat. Methods* **2011**, *8*, 413.
(13) Yu, J.; Liu, G. X.; Sumant, A. V.; Goyal, V.; Balandin, A. A. *Nano Lett.* **2012**, *12*, 1603.
(14) Jung, I.; Field, D. A.; Clark, N. J.; Zhu, Y. W.; Yang, D. X.; Piner, R. D.; Stankovich, S.; Dikin, D. A.; Geisler, H.; Ventrice, C. A.; Ruoff, R. S. *J. Phys. Chem. C* **2009**, *113*, 18480.
(15) Mattson, E. C.; Johns, J. E.; Pande, K.; Bosch, R. A.; Cui, S. M.; Gajdardziska-Josifovska, M.; Weinert, M.; Chen, J. H.; Hersam, M. C.; Hirschmugl, C. J. *J. Phys. Chem. Lett.* **2013**, *5*, 212.
(16) Acik, M.; Lee, G.; Mattevi, C.; Chhowalla, M.; Cho, K.; Chabal, Y. J. *Nat. Mater.* **2010**, *9*, 840.
(17) Ajayan, P. M.; Yakobson, B. I. *Nature* **2006**, *441*, 818.
(18) Sanchez, A.; Mondragon, F. *J. Phys. Chem. C* **2007**, *111*, 612.
(19) Robinson, J. T.; Perkins, F. K.; Snow, E. S.; Wei, Z. Q.; Sheehan, P. E. *Nano Lett.* **2008**, *8*, 3137.
(20) Boukhvalov, D. W.; Katsnelson, M. I. *J. Am. Chem. Soc.* **2008**, *130*, 10697.
(21) Moser, J.; Barreiro, A.; Bachtold, A. *Appl. Phys. Lett.* **2007**, *91*, 163513.
(22) Wang, X. R.; Li, X. L.; Zhang, L.; Yoon, Y.; Weber, P. K.; Wang, H. L.; Guo, J.; Dai, H. J. *Science* **2009**, *324*, 768.
(23) Li, X. L.; Wang, H. L.; Robinson, J. T.; Sanchez, H.; Diankov, G.; Dai, H. J. *J. Am. Chem. Soc.* **2009**, *131*, 15939.
(24) Li, X. L.; Wang, X. R.; Zhang, L.; Lee, S. W.; Dai, H. J. *Science* **2008**, *319*, 1229.
(25) Schwierz, F. *Nat. Nanotechnol.* **2010**, *5*, 487.
(26) Carlsson, J. M.; Hanke, F.; Linic, S.; Scheffler, M. *Phys. Rev. Lett.* **2009**, *102*, 166104.
(27) Wang, X. R.; Ouyang, Y. J.; Li, X. L.; Wang, H. L.; Guo, J.; Dai, H. J. *Phys. Rev. Lett.* **2008**, *100*, 206803.
(28) Deng, S.; Tjoa, V.; Fan, H. M.; Tan, H. R.; Sayle, D. C.; Olivo, M.; Mhaisalkar, S.; Wei, J.; Sow, C. H. *J. Am. Chem. Soc.* **2012**, *134*, 4905.
(29) Yuan, W. J.; Liu, A. R.; Huang, L.; Li, C.; Shi, G. Q. *Adv. Mater.* **2013**, *25*, 766.
(30) Li, J.; Lu, Y. J.; Ye, Q.; Cinke, M.; Han, J.; Meyyappan, M. *Nano Lett.* **2003**, *3*, 929.
(31) Mattson, E. C.; Pande, K.; Unger, M.; Cui, S. M.; Lu, G. H.; Gajdardziska-Josifovska, M.; Weinert, M.; Chen, J. H.; Hirschmugl, C. J. *J. Phys. Chem. C* **2013**, *117*, 10698.
(32) Pagni, P. J.; Keck, J. C. *J. Chem. Phys.* **1972**, *58*, 1162.
(33) Barakat, T.; Abodayeh, K.; Al-Dossary, O. M. *Czech. J. Phys.* **2006**, *56*, 583.
(34) Lin, X. Q.; Ni, J.; Fang, C. *J. Appl. Phys.* **2013**, *113*, 034306.
(35) Cui, S. M.; Pu, H. H.; Mattson, E. C.; Lu, G. H.; Mao, S.; Weinert, M.; Hirschmugl, C. J.; Gajdardziska-Josifovska, M.; Chen, J. H. *Nanoscale* **2012**, *4*, 5887.
(36) Ozaki, T. *Phys. Rev. B* **2003**, *67*, 155108.